J. Fluid Mech. (1994), *vol.* 281, *pp.* 193–218

Experiments in a boundary layer subjected to free stream turbulence. Part 1. Boundary layer structure and receptivity

By K. J. A. WESTIN[1], A.V. BOIKO[2], B. G. B. KLINGMANN[1]†, V.V. KOZLOV[2] AND P. H. ALFREDSSON[1]

[1]Department of Mechanics/Fluid Physics, Royal Institute of Technology, S-10044 Stockholm, Sweden

[2]Department of Theoretical and Applied Mechanics, Russian Academy of Sciences, Siberian Branch, 630090 Novosibirsk, Russia

(Received 17 November 1993 and in revised form 8 July 1994)

The modification of the mean and fluctuating characteristics of a flat-plate boundary layer subjected to nearly isotropic free stream turbulence (FST) is studied experimentally using hot-wire anemometry. The study is focussed on the region upstream of the transition onset, where the fluctuations inside the boundary layer are dominated by elongated flow structures which grow downstream both in amplitude and length. Their downstream development and scaling are investigated, and the results are compared with those obtained by previous authors. This allows some conclusions about the parameters which are relevant for the modelling of the transition process. The mechanisms underlying the transition process and the relative importance of the Tollmien–Schlichting wave instability in this flow are treated in an accompanying paper (part 2 of the present report).

1. Introduction

Despite being a subject of interest since the thirties, the effect of free stream turbulence (FST) on the onset of transition has received detailed attention only in the last few years. This problem is of great interest in applied engineering, for instance for the prediction of transition on turbine blades, where the impingement of turbulence from the wake of the stator influences the boundary layers on the rotor blades. Another important aspect is the influence of FST on wind-tunnel experiments in general (both sub- and supersonic). It is desirable to reduce the FST-level in order to resemble free-flight conditions, but all wind tunnels have some background disturbances with different characteristics, and more knowledge about the 'dangerous' FST-parameters will be of interest. Attempts have been made by several authors to establish empirical correlations between FST and the transition Reynolds number. At FST-levels (Tu) above 5%, transition occurs at the minimum Reynolds number where self-sustained boundary-layer turbulence can exist, i.e. at $Re_\theta \approx 190$ where Re_θ denotes the Reynolds number based on momentum loss thickness (see Arnal 1992, for a review). At lower levels of FST, however, different experiments

† Present address: Volvo Aerospace Corp., Space Propulsion Division, S-461 81 Trollhättan, Sweden.

disagree widely as to the location and extent of the transition region, and there seems to be no general correlation between the level of the FST and the location of transition onset. Neither can the transition Reynolds number be found by merely taking into account the fluctuations inside the boundary layer. Transition is also sensitive to a large number of other parameters, including not only the overall level of FST but also spatial scales, degree of isotropy and homogeneity, conditions at the leading edge of the model, presence of pressure gradients, etc., each of which requires special attention. Depending on these conditions, the transition process may be dominated by Tollmien–Schlichting (TS) waves, algebraic transient growth or other as yet unknown instabilities, which require different modelling approaches. The basic problem in modelling FST-induced transition, as pointed out by Arnal, is the lack of understanding of the transition mechanisms at work.

For engineering purposes, recent attempts have been made to model transition in the presence of FST by transport equations. Most transport models rely on a transition criterion, usually derived from an empirical correlation, for modifying the closure parameters through the transition region. If transition is to be modelled without resorting to empirical correlations, it is necessary to correctly reproduce the laminar flow characteristics upstream of the onset of transition. An extensive comparison of numerical methods, using the experiments by Roach & Brierley (1992) as a reference (the so-called T3 test cases), was made during the 'Workshop on Transition and Turbulence in Lausanne' (see Pironneau *et al.* 1992). From the results presented at this Workshop, it seems that transport models can barely reproduce the structure of the laminar boundary layer fluctuations needed for the closure of the equations.

So far, only a few experimental studies have reported measurements of the mean velocity in the region upstream of transition for boundary layers subjected to FST. Nor have comparisons been made between fluctuation characteristics obtained in different experiments, despite the fact that such experimental data usually are presented. Because of the lack of knowledge about the effect of different parameters involved, it is necessary to be careful when drawing conclusions from results obtained under different experimental conditions. In the present experiments, special care was taken to create 'standard' experimental conditions: a zero pressure gradient, control of leading edge conditions, isotropy of the grid-generated turbulence, and a low level of uncontrolled free stream disturbances (both sound and turbulence).

This paper is organized as follows. A brief overview of previously known results on the receptivity of the boundary layer to FST is given below. The experimental set-up is described in § 2, and the free stream characteristics are discussed in § 3. Results of investigations of the boundary layer structure are presented in § 4, and discussed in section 5 together with previous author's findings. The main conclusions from this study are summarized in § 6.

1.1. *Brief overview of the boundary layer receptivity to FST*

The first detailed measurements concerning the development of a laminar boundary layer in the presence of FST were presented by Arnal & Juillen (1978). They observed a downstream growth of the streamwise velocity fluctuations (u_{rms}), reaching amplitudes of several percent of the free stream velocity (U_0) before the onset of transition. They also found that the energy spectrum inside the boundary layer is dominated by contributions at much lower frequencies than in the turbulent free stream. The distribution of u_{rms} across the boundary layer was quite different from that of TS-waves (e.g. the maximum was found near the middle of the boundary layer

instead of near the wall as for TS-waves). Waves with frequencies typical of unstable TS-waves were also seen riding on the large-scale (low-frequency) structures; however, their amplitudes were small compared with the overall fluctuation level. Later studies by Kendall (1985, 1990, 1991) were focussed on the receptivity and development of wave packets induced by FST at Tu between 0.1% and 0.2%. At higher disturbance levels the TS-waves become difficult to detect, and their role in transition is therefore not clear. Recent experiments by Blair (1992), carried out in accelerating flows at a high ambient disturbance level, show that transition can also occur under conditions which are subcritical with respect to TS-waves.

The boundary layer perturbations were investigated at larger FST levels in experiments by Kosorygin *et al.* (1982) and Kosorygin & Polyakov (1990), who found that the shape of the u_{rms}-profile is nearly independent of both Tu and the Reynolds number. The spanwise and wall-normal scales of the low-frequency structures were of the order of the boundary layer thickness, and the amplitude of normal velocity fluctuations (v_{rms}) inside the boundary layer was several times smaller than u_{rms}. Flow visualizations (Kendall 1985; Gulyaev *et al.* 1989) show that the low-frequency fluctuations in the boundary layer are caused by longitudinal streak structures which start to develop from the leading edge of the plate. It should be emphasized that the observed boundary layer perturbations with a dominating streaky pattern, although random in time and space, are not what we usually call turbulence.

Neither the receptivity nor the growth mechanism of the observed longitudinal structures have so far been identified, and their precise role in the transition to turbulence is not clear. They are sometimes referred to as 'Klebanoff modes', due to early (unpublished) observations by P.S. Klebanoff. More recently, Herbert (1993, see also Herbert, Stuckert & Esfahanian 1993) has interpreted them as a result of algebraic growth of transient disturbances. As opposed to discrete instability modes (such as TS-waves), the algebraic growth is strongly dependent on the forcing disturbances, resulting in a receptivity problem rather than a stability problem.

Experimentally, the receptivity of the boundary layer to free stream disturbances can be investigated by generating controlled 'model' disturbances in the free stream, and studying the subsequent development of perturbations inside the boundary layer. Such experiments by Grek, Kozlov & Ramazanov (1985) and Grek *et al.* (1991) have shown that a transient localized disturbance upstream of the leading edge can initiate the development of unstable flow structures in the boundary layer in the same way as transient disturbances introduced from the wall or in the interior of the boundary layer. After an initial development, these structures develop into turbulent spots, provided that the initial disturbance is large enough. 'Incipient spots' have been extensively studied theoretically, experimentally and numerically (cf. Breuer & Landahl 1990; Grek *et al.*; Klingmann 1992; Henningson, Lundbladh & Johansson 1993). They are characterized by algebraic energy growth, and are dominated by streaky structures elongated in the streamwise direction, where the lateral scale of the streaks is fairly constant when moving downstream.

Suder, O'Brien & Reshotko (1988) and Roach & Brierley (1992) directed their attention to the transition region itself. In the experiments by Suder *et al.*, transition was observed at remarkably low Reynolds numbers compared with other experiments made under similar conditions, and turbulent spots appeared at relatively low fluctuation levels in the boundary layer (3–4% of U_0). The onset of turbulence is accompanied by a rather sharp increase in the wall shear stress, and can also be clearly seen in the fluctuating velocity profiles, which develop a distinct near-wall maximum due to the turbulent motion. Irrespective of the dominant mechanism responsible

for the transition, which may have been different in all the above mentioned cases, the transition region is characterized by a random appearance of turbulent spots which grow in number and size downstream, until the boundary layer becomes fully turbulent.

A critical part of the experimental set-up is the leading edge of the plate, where a slightly non-uniform pressure distribution at the leading edge can have a substantial effect on TS-wave amplification (see Klingmann *et al.* 1993). The effect of different leading edge bluntness in the presence of FST was investigated by Kendall (1991). It was found that the amplitude of waves in the TS-wave frequency band was much higher in the case of a blunt leading edge, while the amplitude of the low-frequency perturbations was not affected. The generation of turbulent spots at the leading edge is also affected by the shape and the pressure distribution at the leading edge, where small (unstationary) separation bubbles will favour the formation of turbulent spots. This was studied in an experiment by V. E. Kozlov *et al.* (1990), where local separation was attenuated by a small negative angle of attack, resulting in a downstream movement of the transitional Reynolds number. By rounding the leading edge, the same effect could be obtained at a smaller negative angle of attack.

An observation made at the Lausanne Workshop is the sensitivity to the specified free stream characteristics. The structure of grid-generated FST depends on the free stream velocity and flow quality upstream of the grid, the grid geometry, as well as on how the grid is installed. In most transition experiments, the turbulence level is described in terms of the r.m.s.-level and the spectral distribution of the streamwise velocity component (u) in the free stream. In a numerical study by Yang & Voke (1991), different free stream conditions were imposed, and it was found that free stream fluctuations in the pressure (p) and normal velocity (v) are the most efficient in exciting perturbations in the boundary layer, whereas fluctuations in the streamwise velocity (u) are rather harmless. Unless the FST is isotropic, the scales and intensity of the v-component cannot be obtained from the frequency spectrum of u. If the grid is installed in the settling chamber, as in the experiments of Kendall (1985, 1990, 1991) and Suder *et al.* (1988), the streamwise fluctuations are suppressed more efficiently than the transverse fluctuations when the flow passes through the contraction. This gives an anisotropy in the FST, which decays along the test section. In such a case, it is necessary to study the cross-stream scales, in order to asses the precise characteristics of the FST.

2. Experimental set-up and measurement technique

The experiments were performed in the MTL (Minimum Turbulence Level) wind tunnel at the Royal Institute of Technology (KTH), Stockholm, Sweden. It is a closed return tunnel, with a 7 m long test section of 0.8 × 1.2 m cross-section, preceded by a contraction with ratio 9:1. One of the particular features of this tunnel is the low level of free stream turbulence in the test section, where the intensity of the streamwise velocity fluctuations is below 0.02% in the velocity interval 10–60 m s^{-1} (see Johansson 1992). This can be regarded as an upper limit, since the tunnel turbulence tends to decrease as the velocity decreases. The experimental set-up as well as the measurement parameters are matched to the experiments by Klingmann *et al.* (1993) for an undisturbed flat-plate boundary layer flow at zero pressure gradient – in fact some of the measurements were carried out simultaneously.

A general sketch of the set-up is shown in figure 1. The experiments were carried out on a 2.16 m long flat plate (called set-up I) or a 4.22 m long plate (set-up II). Set-up I

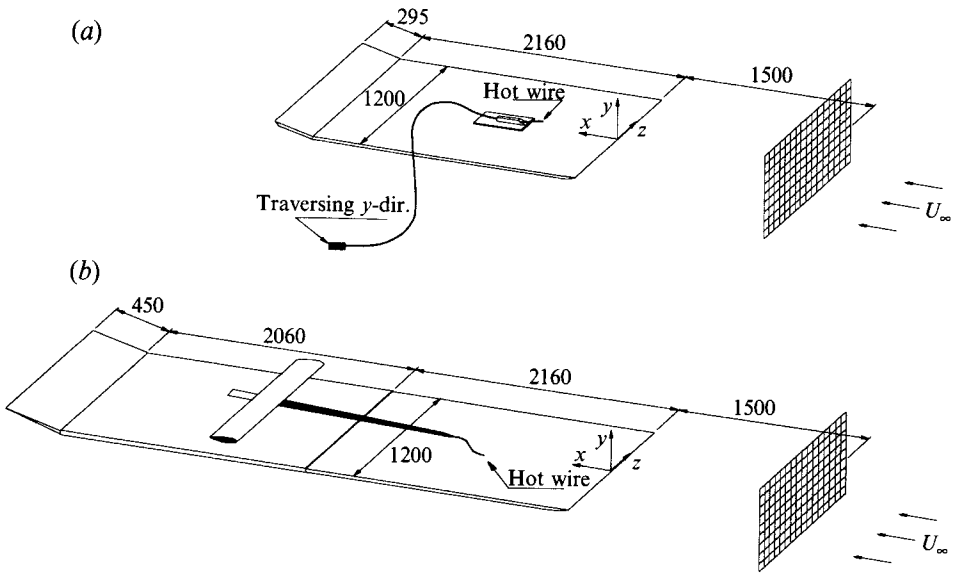

FIGURE 1. Outline of experimental set-up: (*a*) set-up I, (*b*) set-up II. Dimensions in mm.

is identical to that described in Klingmann *et al.* (1993). The streamwise, wall-normal and spanwise directions are denoted x, y and z respectively. Measurements were undertaken in the region between 100 and 1000 mm from the leading edge ($x = 0$), at free stream speeds (U_0) between 4 m s^{-1} and 8 m s^{-1}. The Reynolds number, defined as $R = 1.72(U_0 x/\nu)^{1/2}$ where ν is the kinematic viscosity, was between 200 and 1260.

FST was generated by a grid, installed in the test section 1.5 m upstream of the leading edge of the plate. The mesh size and the wire diameter of the grid were 23.5 mm and 3.5 mm respectively, giving a solidity of 0.28 (the solidity is defined as the grid blockage area over the total area). This resulted in a fairly isotropic turbulence with a level of Tu about 1.5%. A detailed description of the grid-generated turbulence is given in § 3. With the grid installed, turbulent spots were occasionally observed at $x = 1000$ mm and $U_0 = 8$ m s^{-1}. This position can be said to correspond to the beginning of the transition region.

The streamwise and normal velocities were measured with constant-temperature hot-wire anemometers, using both single and cross-wire probes. The single wires were made of 5 μm platinum wire with a sensing length of 1 mm, operating at 60% overheat, and calibrated with a Prandtl tube in the free stream. A calibration function of the form

$$U = k_1(E^2 - E_0^2)^{1/n} + k_2(E - E_0)^{1/2}$$

was used, where E and E_0 are the anemometer output voltages at the velocities U and zero respectively, and k_1, k_2 and n are constants to be determined for the best fit to the calibration data. The value of n is usually close to 0.5. The second term represents the contribution from free convection at low velocities, and makes it possible to extrapolate the calibration curve to low velocities. A cross-wire probe, used for measurements of both the streamwise and transverse velocity components in the free stream, was made of 2.5 μm wires and had a measurement volume smaller than 0.5 mm in side length. The probe was calibrated at different angles and flow velocities, from which u and v were calculated, and a voltage pair (E_1, E_2) was obtained

at each calibration point. Two third-degree polynomial surfaces were then fitted to the calibration data, giving u and v as functions of (E_1, E_2).

Temperature variations within 1° were accounted for by compensating the output voltage from the anemometer by a factor

$$E_{corr} = \frac{E}{[1 - \Delta T/(T_s - T_f)]^{1/2}}$$

where E and E_{corr} denote the measured and corrected voltages respectively, T_s is the sensor temperature, T_f is the fluid temperature and ΔT is the temperature drift.

The probes were traversed in the following two different ways. In set-up I the probe was supported by an 82 mm long rod and was traversed in the y-direction (normal to the wall) by means of a wedge mechanism moveable with a micrometer screw and operated via a speedometer wire from outside the tunnel. The accuracy of the hot-wire position with this mechanism was about 0.02 mm. In some later measurements (set-up II) a newly constructed traversing mechanism made it possible to traverse the probe in all three directions with an accuracy of 0.01 mm. This system was used for all X-wire measurements. In set-up II, the flat plate was prolonged with a 2 m long extension plate, in order to avoid interference between its trailing edge flap and the traversing mechanism. The length of the sting in this set-up was approximately 1700 mm, and consequently vibrations were observed with an eigenfrequency of 20 Hz. With the probe positioned in the linear region of the boundary layer close to the wall at $x = 1000$ mm, the vibrations resulted in a r.m.s.-value of approximately 0.14% of U_0 in the 20 Hz component. The effect of the vibrations is larger for positions further upstream, and the possible influence will be discussed in connection with the results.

2.1. *Leading edge conditions and pressure distribution over the plate*

The leading edge of the flat plate is one of the critical points in the design of the experiment, since the pressure conditions there may influence both the boundary layer development and the receptivity. A uniform pressure distribution near the leading edge cannot usually be obtained using elliptic or wedge-shaped leading edges, although careful attention to this problem can minimize undesirable effects. In the present set-up, a smooth pressure distribution was achieved by a special design of the leading edge in combination with a trailing edge flap for adjustment of the stagnation line (see also Klingmann *et al.* 1993).

The importance of leading edge effects can be appreciated from a simple observation made during the preparations of the experiment: when the trailing edge flap was lowered, the stagnation point moved to the reverse side of the plate, resulting in a strong suction peak on the working side. The peak level was about 10% of the dynamic pressure, and affected the region $x < 200$ mm. With the grid installed, the flow was then already fully turbulent at $x = 500$ mm and $U_0 = 8$ m s^{-1}. After adjustment of the flap, the transition point was moved downstream of the last measurement position ($x = 1000$ mm).

The flat plate is a sandwich construction with a total thickness of 19 mm, which was installed horizontally at a height of 160 mm from the test section floor measured close to the leading edge, giving a distance of 635 mm between the tunnel top wall and the working surface of the plate. The working side consists of a 6 mm thick plate of cast, milled and polished aluminium. The plate is equipped with a 158 mm long asymmetric leading edge, shown in figure 2*a*. The shape of the leading edge was designed so as to minimize the pressure gradients on the working side in the region near the stagnation line. (This was done using two-dimensional potential flow

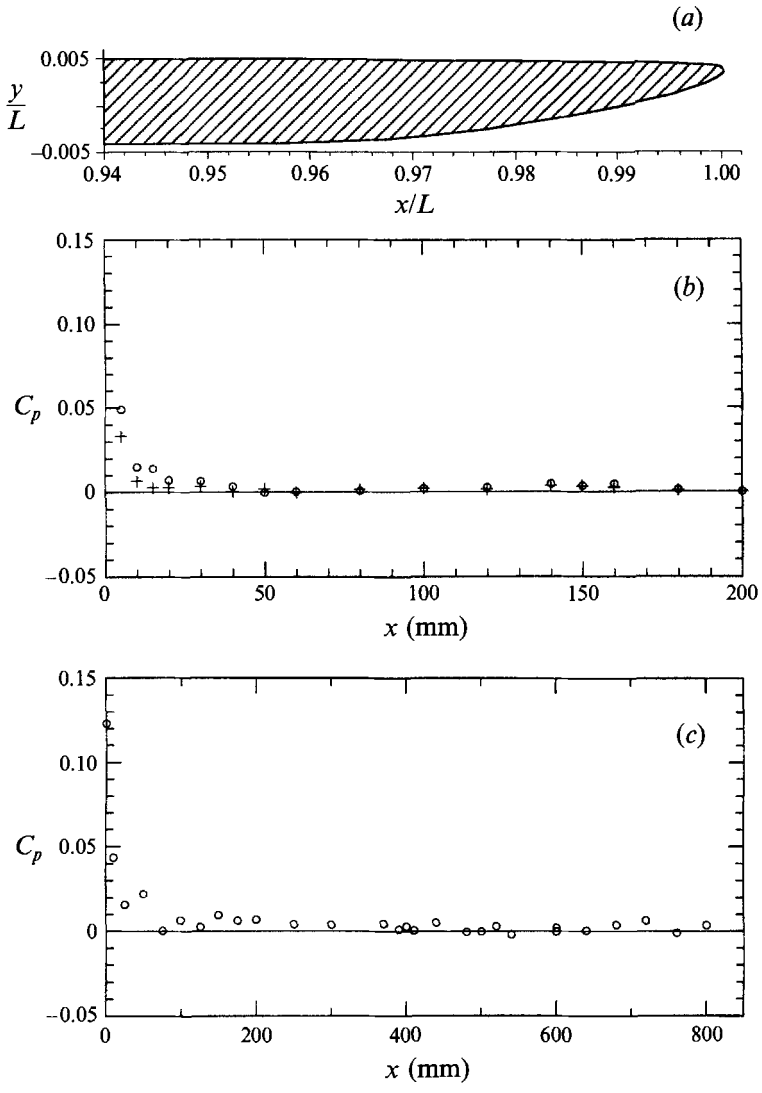

FIGURE 2. (*a*) Leading edge of the flat plate. Reference length $L = 2$ m. (*b*) Distribution of the pressure coefficient (C_p) close to the leading edge: with the grid installed (+), without grid (○). Reference position $x = 200$ mm. (*c*) Pressure distribution along the plate. Ref. position $x = 500$ mm.

calculations, where the presence of the top and bottom walls of the test section was taken into account.)

The test section walls were adjusted to obtain a zero streamwise pressure gradient along the plate, and thereafter the trailing edge flap was used to adjust the stagnation line on the leading edge. Figures 2(*b*) and 2(*c*) show the pressure distribution with and without the grid near the leading edge and along the working part of the plate after adjustment of the flap. The pressure coefficient is defined as

$$C_p = \frac{p - p_{ref}}{p_0 - p_{ref}}$$

where p is the local static pressure, p_{ref} the static pressure at a reference point on the plate and p_0 the total pressure (note that with this definition, $C_p = 1$ on the

stagnation line). It was obtained by measuring U_0 near the edge of the boundary layer, and then evaluating the pressure from Bernoulli's equation (this procedure was found to be more accurate than measuring the static pressure directly). The pressure decreases smoothly within the first 20 mm, as the flow accelerates from the stagnation point (see figure 2*b*), without producing a suction peak. Downstream of $x = 20$ mm, C_p is constant to within 1%. Compared with set-ups reported in other studies, the departure from a perfect zero pressure gradient near the leading edge is quite small, and it is also confined to a smaller region. For reference, in the set-up of Arnal & Juillen (1978) the leading edge of their body of revolution caused an accelerating flow in the first 150 mm, followed by a small positive pressure gradient along the model (about 4%/m). Roach & Brierley (1992) report pressure deviations amounting to about 3% on the wedge-shaped leading edge used in their experiment, and similar deviations were reported in the experiments by Suder *et al.* (1988). In the latter experiment the test section floor was used as flat plate, and a boundary layer bleed scoop served as the leading edge. However, neither Roach & Brierley nor Suder *et al.* report the pressure distribution close to the leading edge (the most upstream pressure taps were positioned at 50 mm and 80 mm respectively).

The presence of the grid tends to decrease the pressure and thereby enhance the tendency for the formation of a suction peak near the leading edge. In the present set-up, the grid is seen to give a small decrease in the pressure ($\Delta C_p < 1.5\%$) within the first 20 mm from the stagnation line (see figure 2*b*), while the pressure distribution further downstream is unaffected by the grid. It should be emphasized that the position of the flap was the same both with and without the grid installed.

3. Characteristics of the free stream turbulence

In order to investigate the boundary layer receptivity, it is necessary to have a good characterization of the FST. Its structure depends on several parameters, for instance the free stream velocity and flow quality upstream of the grid, the geometry of the grid and how it is installed. The low level of background turbulence and sound in the MTL wind tunnel allows a good control of the free stream conditions. The grid was placed in the test section, 60 mesh widths upstream of the flat plate leading edge. Grid-generated turbulence is usually assumed to become isotropic after 20 mesh widths; however, some studies indicate that a small anisotropy may survive over 400 mesh widths downstream (see Groth & Johansson 1988 for a more extensive discussion), and this was also found to be the case in the present set-up. This affects the ratios between u and v, and between the transverse and longitudinal turbulent scales. The interest is here focussed on the Taylor microscale and the integral scale, which may be assumed to be the most relevant for the boundary layer receptivity.

The turbulence level Tu is here defined as $u_{rms,0}/U_0$, where $u_{rms,0}$ is the r.m.s.-level of u in the free stream, measured close to the leading edge ($x = 0$). Tu was 1.5% at $U_0 = 8$ m s^{-1} and 1.35% at $U_0 = 4$ m s^{-1}, and its variation with U_0 was approximately linear within this velocity range. Figure 3(*a*) shows the spectral density of u for $U_0 = 4$ and 8 m s^{-1}, plotted versus the non-dimensional frequency F, defined as $2\pi f\nu \times 10^6/U_0^2$. The spectral density ($E$) is here defined as the spectral power normalized by $0.5U_0^2\Delta F$ (ΔF is the frequency resolution), and is therefore independent of the sampling parameters. From figure 3(*a*) it is clear that the relative energy distribution is shifted slightly towards higher F when the velocity is decreased. The turbulent scales can be compared by looking at the autocorrelations of u (R_{uu}) for the two velocities (figure 3*b*). Using Taylor's hypothesis, the time separation (Δt)

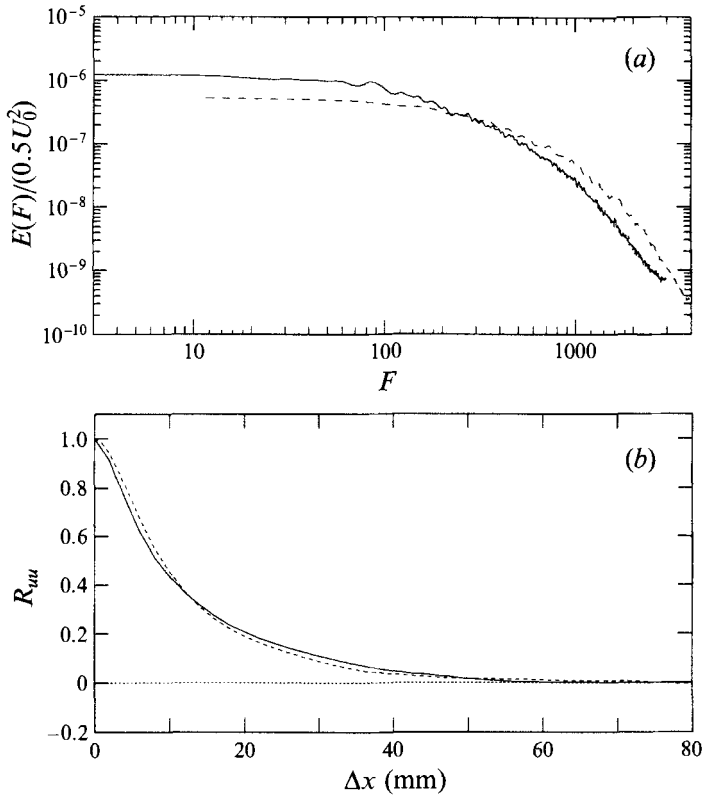

FIGURE 3. (*a*) Free stream spectra and (*b*) autocorrelation of u at $x = 0$. $U_0 = 4\ \mathrm{m\,s^{-1}}$ (– – –), $U_0 = 8\ \mathrm{m\,s^{-1}}$ (——).

was translated into a longitudinal space separation (Δx) by multiplication with U_0. The correlation functions are quite similar for both velocities, indicating that there are only minor differences in the turbulent scales.

Figure 4(*a*) compares the spectral density of the u- and v-fluctuations in the free stream, measured with an X-wire probe at $x = 0$ and $U_0 = 8\ \mathrm{m\,s^{-1}}$. In agreement with the theory for isotropic turbulence, the energy of u is shifted to lower frequencies than the v-spectrum. In order to assess the degree of isotropy and the typical transverse scales in the free stream, the FST was investigated in more detail at $U_0 = 8\ \mathrm{m\,s^{-1}}$. A relevant test of the isotropy of the scales is to compare the spatial correlations in different directions. Two-probe cross-correlations of u were measured in the free stream at $x = 500$ mm, using separations in both y and z. This gives the transversal correlation in the crossflow directions. These results are shown in figure 4(*b*) together with the autocorrelation of v, obtained from the frequency spectrum. By using Taylor's hypothesis, the autocorrelation curve can be interpreted as a transversal correlation in the streamwise direction. The good agreement between the three correlation curves shows that the fluctuation scales are near isotropic. The autocorrelation of u, which is the same as shown in figure 3(*b*), is also plotted for reference.

The turbulent microscale τ (Taylor timescale) gives an estimate of the smallest energetic eddies in the turbulence. It can be estimated directly from the autocorrelation, but here it was calculated as the ratio between the turbulent r.m.s.-fluctuations and

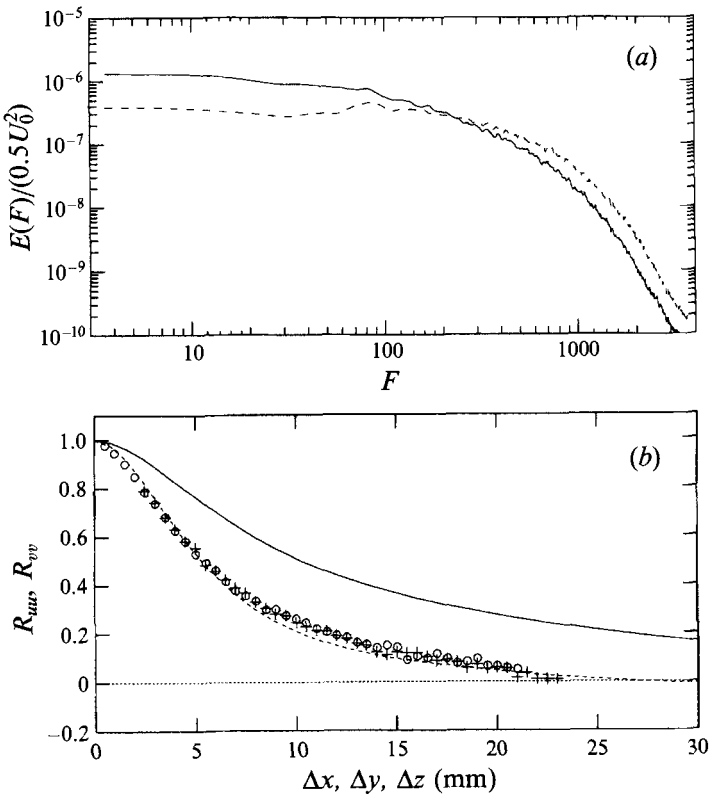

FIGURE 4. (*a*) Free stream spectra at $x = 0$, $U_0 = 8$ m s^{-1}. u- (—) and v-component (– – –). (*b*) Free stream correlations at $x = 500$ mm, $U_0 = 8$ m s^{-1}. Autocorrelation of u- (—) and v-component (– – –). Cross-correlations with Δy (○) and Δz (+) probe separations.

their time derivatives,

$$\tau_u = \sqrt{2}\frac{u_{rms}}{(\partial u/\partial t)_{rms}}$$

and similarly for the v-component. This expression can be derived from a Taylor series expansion of the correlation function (cf. Hinze 1975). $\partial u/\partial t$ was approximated by $\Delta u/\Delta t$ and successively decreasing Δt (increasing the sampling frequency) until a limit was reached where cancellation effects became visible. τ_u^2 was then obtained from extrapolation to the limit $\Delta t \to 0$, by fitting a second-degree polynomial to τ_u^2 as a function of Δt. At $x = 0$, the longitudinal and transverse microscales were calculated to $\tau_u = 0.87$ ms and $\tau_v = 0.57$ ms ($U_0 = 8$ m s^{-1}), which gives a ratio of 1.53. The theoretical ratio for isotropic turbulence is $\sqrt{2} = 1.41$. The corresponding transverse lengthscale (λ_v) is 4.6 mm. As a consequence of the dissipation of the smallest scales, the lengthscales increase downstream. At $x = 500$ and 1000 mm, the values of λ_v are 5.2 and 5.9 mm respectively.

The integral lengthscales (Λ_u and Λ_v), are usually calculated by integrating the autocorrelation functions shown in figure 4(*b*) over all separations. However, the integrated values are often ambiguous, because the autocorrelation curve is easily affected by long time fluctuations in the mean velocity, resulting in different integral lengthscales depending on the chosen sampling parameters. This problem is most evident in the u-correlation. Another possibility is to extrapolate the energy density

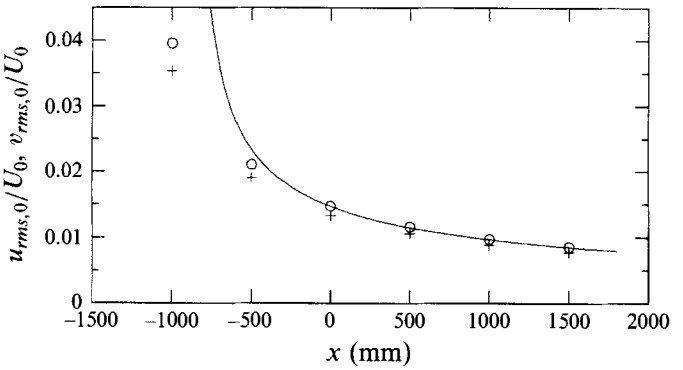

FIGURE 5. Downstream decay of FST for $U_0 = 8$ m s^{-1}. $u_{rms,0}/U_0$ (○), $v_{rms,0}/U_0$ (+), decay curve according to $u_{rms,0}/U_0 = C(x - x_0)^b$ with $b = -0.54$, $x_0 = -871$ mm (—).

spectra $E(F)$ to $F = 0$. The integral timescale is then obtained as $E(0)$ normalized with u_{rms}^2, but also with this method there is a significant arbitrariness when the extrapolation is carried out. By extrapolating the v-spectra, Λ_v was estimated to be within 7–10 mm along the flat plate, and the corresponding Λ_u was 2 to 3 times larger. The rather small ratio between integral and micro scales (Λ_v/λ_v) may be explained by the small turbulent Reynolds number ($Re_\lambda = u_{rms}\lambda_v/\nu \approx 40$).

The downstream development of the free stream fluctuations ($u_{rms,0}$ and $v_{rms,0}$) are shown in figure 5. The typical power-law decay can be described in the form

$$\frac{u_{rms,0}}{U_0} = C(x - x_0)^b,$$

where x_0 is a virtual origin. A curve fit of this form to the data measured at $x \geqslant 0$ gave an exponent $b = -0.62$, in fair agreement with other investigations of grid-generated turbulence, e.g. Baines & Petersen (1951) obtained $b = -0.71$ ($-5/7$) and Groth & Johansson (1988) $b = -0.5$. If it is assumed that the decaying turbulence can be described by the k-ϵ model, the exponent can easily be derived if the turbulent diffusion terms are neglected. This would give an exponent of -0.54 for the empirical coefficient $c'_{\epsilon 2} = 1.92$ ($b = 0.5/(1 - c'_{\epsilon 2})$). A smaller exponent is obtained if data measured upstream of the leading edge are included, since these are more affected by the anisotropic region near the grid. The ratio between $v_{rms,0}$ and $u_{rms,0}$ has an approximately constant value of 0.9 along the measured region, indicating a minor degree of anisotropy. For comparison, in the experiments of Roach & Brierley (1992), this ratio was reported to be equal to 1 to within 0.5%.

In summary, despite the good agreement between the correlations in all three transverse directions (figure 4*b*), careful inspection of the parameters studied above (i.e. the ratios $v_{rms,0}/u_{rms,0}$ and τ_u/τ_v, as well as the exponent b), reveals a minor degree of anisotropy in the present set-up. At 8 m s^{-1}, typical transverse scales in the free stream range between 4.6 mm (Taylor's microscale) and 10 mm (integral or macro scale). At 4 m s^{-1}, the value of Tu is almost the same. By comparing the autocorrelations of u at 4 and 8 m s^{-1} (see figure 3*b*), the turbulence scales are estimated to be approximately equal at both velocities. On the other hand, the boundary layer thickness at a given R is $\sqrt{2}$ times larger at 4 m s^{-1} than at 8 m s^{-1}. This means that the relative size of the free stream eddies compared with the boundary layer thickness are smaller at 4 m s^{-1}, a factor which may be of importance for the receptivity of the boundary layer to free stream disturbances.

x (mm)	U_0 (m s^{-1})	δ^* (mm)	$\delta^*/(\nu x/U_0)^{1/2}$	Re_{δ^*}	$1.72Re_x^{1/2}$	H
450 without grid	4.1	2.27	1.77	623	605	2.58
450	4.0	2.23	1.71	587	592	2.55
450 without grid	8.0	1.560	1.70	827	840	2.58
450	8.1	1.553	1.70	834	846	2.53

TABLE 1. Boundary layer characteristics

4. Structure of the boundary layer perturbations

In this section we will describe the effect of FST on the mean and fluctuating velocities upstream of the onset of transition. Results from measurements at different R are presented and compared, allowing some conclusions to be drawn about the downstream development and scaling of the perturbations induced by FST. The measurements at 4 m s^{-1} were made in set-up I, which is identical to that reported by Klingmann *et al.* (1993), whereas the measurements for 8 m s^{-1} were obtained in set-up II. At far downstream positions, turbulent spots occurred occasionally. Since the objective of the present study is to document the laminar boundary layer development, sampling records affected by the passage of turbulent spots were rejected.

4.1. *Mean velocity characteristics of the boundary layer subjected to free stream turbulence*

Mean velocity profiles were measured with an equidistant y-step of 0.1 mm. The distance between the surface and the first y-position was estimated by linear extrapolation of the near-wall part of the profile, after discarding points visibly affected by heat conduction to the wall. The boundary layer characteristics (i.e. the displacement thickness δ^*, the momentum loss thickness θ, and the shape factor $H = \delta^*/\theta$) were then evaluated by numerical integration according to Simpson's formula. The accuracy in the value of H obtained from this procedure was estimated to be within $\pm 0.5\%$, but this error does not include possible inaccuracies in the hot wire calibration. Comparisons between profiles measured with different calibrations indicated that the inaccuracy in the evaluation of H may be slightly larger. However, this error limit is well below the observed differences between the cases with and without a grid.

Figures 6(*a*) and 6(*b*) compare boundary layer profiles measured with and without the grid at $x = 450$ mm. The y-coordinate is normalized with the measured value of δ^*, given in table 1, where we also list the shape factors evaluated from the measured profiles and the ratio between δ^* and $(\nu x/U_0)^{1/2}$. For an ideal Blasius flow this ratio is 1.72, and $H = 2.59$. The undisturbed boundary layer has characteristics close to an ideal Blasius flow, whereas the boundary layer subjected to FST shows small but significant deviations.

The difference between the velocities measured with and without the grid ($\Delta U/U_0$) at $x = 450$ mm are shown in figures 6(*c*) and 6(*d*), and it amounts to about $\pm 1\%$. At both free stream velocities, the presence of the grid gives profiles with larger mean velocity close to the wall, whereas there is a velocity deficit in the outer part of the boundary layer. The perturbed profile is qualitatively similar to a Falkner–Skan (FS) profile for a negative pressure gradient. In figure 6(*c,d*) the measured deviations are compared with the difference between a Falkner–Skan profile and a Blasius profile, where the FS profile was chosen to have the same shape factor as the measured profile (for more details, see the Appendix). It can be seen that the measured deviations are

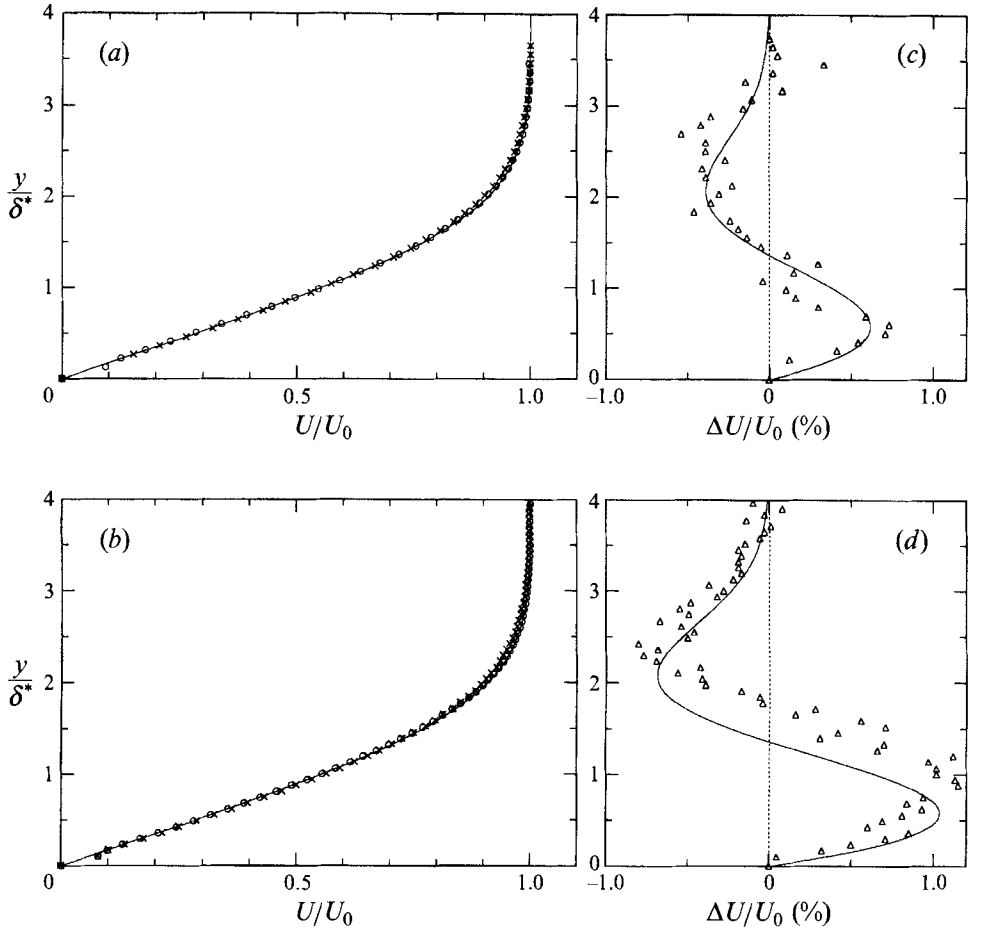

FIGURE 6. Mean velocity profiles at $x = 450$ mm for (*a*) $U_0 = 4\ \mathrm{m\,s^{-1}}$ and (*b*) $U_0 = 8\ \mathrm{m\,s^{-1}}$: with grid (×), without grid (○). Solid lines are Blasius profiles. Velocity changes (ΔU) due to free stream turbulence at $x = 450$ mm for (*c*) $U_0 = 4\ \mathrm{m\,s^{-1}}$ and (*d*) $U_0 = 8\ \mathrm{m\,s^{-1}}$. Solid lines show the difference between Falkner–Skan (with same shape factor as measured profile) and Blasius profiles.

found further out in the boundary layer, which means that the skin friction is lower than that for the FS profile. This was found to be a general trend at all Reynolds numbers studied.

The downstream development of the mean velocity profile at $8\ \mathrm{m\,s^{-1}}$ is shown in figure 7(*a*), together with the corresponding Blasius profiles. Three different x-positions are shown: $x = 100$, 500 and 1000 mm. A systematic development towards a fuller profile can clearly be observed, whereas the boundary layer thickness is only slightly affected. The maximum in $\Delta U/U_0$ increases with R, and amounts to 3–4% at $x = 1000$ mm. Figure 7(*b*) shows profiles of ΔU normalized with its minimum value. It can be seen that the shape of ΔU is fairly self-similar at all measured stations. With the present scaling integration of ΔU over the boundary layer thickness will give a zero value; however, as seen from table 1 and table 2 the FST does not significantly change the mass flow in the boundary layer compared with a Blasius profile.

The values of H corresponding to figure 7 are given in table 2, and their variation with R is plotted in figure 8, showing that the shape factor decreases in linear

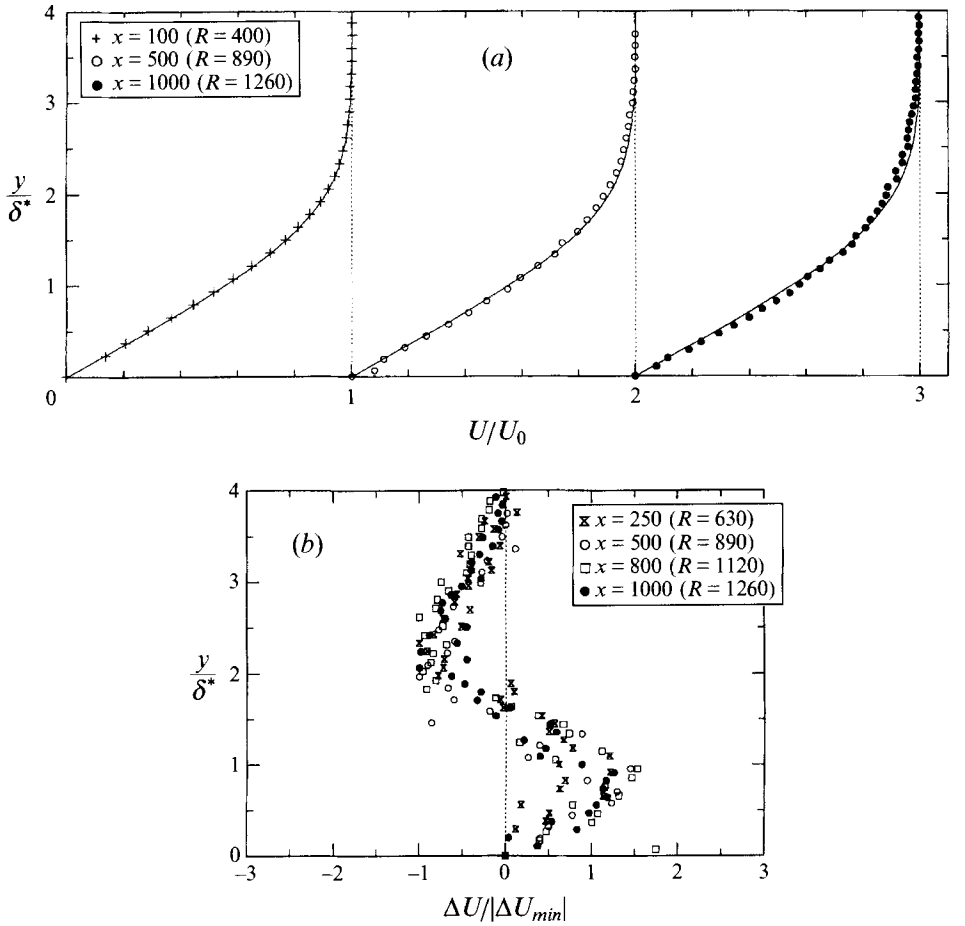

FIGURE 7. (*a*) Mean velocity profiles with grid at $U_0 = 8$ m s^{-1}. Solid lines are Blasius profiles. (*b*) Normalized mean velocity deviations compared with Blasius.

proportion to R. The slope is the same both at 4 m s^{-1} and 8 m s^{-1}, suggesting that the downstream evolution of H may be insensitive to the details of the free stream conditions. The changes in H are mainly due to a downstream increase in θ in comparison with the Blasius case, whereas the ratio between δ^* and $(\nu x/U_0)^{1/2}$ is fairly constant (see table 2). This would not be the case if the deviations were caused by a negative pressure gradient. The downstream development of H at 8 m s^{-1} is equivalent to the effect of an almost constant negative pressure gradient of $\partial C_p/\partial x = -0.16$ m^{-1} for $x > 200$ mm. (This result was obtained by calculating the FS profiles corresponding locally to each H-value and δ^*, see the Appendix.) However, figure 2(*c*) shows that the actual pressure distribution over the plate is constant, so the changes in H cannot be attributed to a pressure gradient. A more plausible explanation, first suggested by Arnal & Juillen (1978), is that the unsteady boundary layer perturbations give rise to Reynolds stresses, which affects the downstream development of the mean flow.

Although the value of H at $R = 1260$ ($x = 1000$ mm) is as small as 2.41, this point can still be considered as upstream of the onset of transition, even though turbulent spots occur occasionally. It should be noted that the deviation from the Blasius flow

x (mm)	U_0 (m s^{-1})	δ^* (mm)	$\delta^*/(\nu x/U_0)^{1/2}$	Re_{δ^*}	$1.72Re_x^{1/2}$	H
100	8.0	0.715	1.65	381	397	2.61
250	8.0	1.125	1.64	600	628	2.54
500	8.0	1.573	1.62	839	888	2.48
800	8.0	2.044	1.66	1090	1124	2.43
1000	8.0	2.251	1.64	1200	1256	2.41

TABLE 2. Boundary layer characteristics

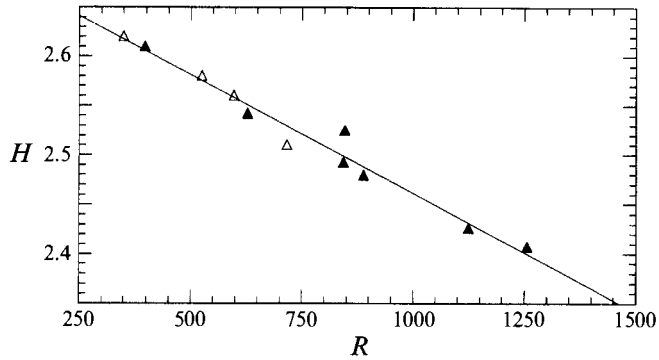

FIGURE 8. Downstream development of the shape factor H. $U_0 = 4$ m s^{-1} (△), $U_0 = 8$ m s^{-1} (▲).

is not due to turbulent intermittency, but reflects the motion of large-scale structures embedded in the boundary layer. The clear difference between these non-turbulent structures and turbulent spots will become evident from the study of the boundary layer fluctuations in the following subsection.

4.2. *Fluctuating velocity*

In order to gain more insight into the nature of the boundary layer perturbations caused by FST, the u-fluctuations were analysed at several downstream positions and for two different free stream velocities. Figure 9(*a*) shows profiles of u_{rms} for $U_0 = 4$ m s^{-1}. Near the boundary layer edge, the amplitude is approximately equal to that in the free stream, and it decreases slowly from 1.35% at the leading edge to 1.1% at $x = 650$ mm ($R = 715$). In contrast, inside the boundary layer the fluctuations are several times larger, and they increase with downstream distance to a value of about 5% at $R = 715$. The r.m.s.-profile scales approximately with δ^*, and its maximum ($u_{rms,max}$) is near $y/\delta^* = 1.4$. At 8 m s^{-1} and $Tu = 1.5\%$ (figure 9*b*), the shape of the r.m.s.-profile is similar, but with the maximum slightly closer to the wall, $y/\delta^* = 1.3$. While the r.m.s.-value in the free stream is slowly decreasing (cf. figure 5), the boundary layer fluctuations increase to almost 11% at $x = 1000$ mm ($R = 1260$). The variation of $u_{rms,max}/U_0$ with x is shown in figure 10 for both velocities. It can be seen that $u_{rms,max}$ varies in linear proportion to R, but the slope is different for the two cases. Also, if $u_{rms,max}$ is scaled with Tu and U_0, there is a larger growth rate for the higher free stream velocity. This may indicate a change in the receptivity to FST when the free stream velocity is changed, due to a change in the relative size of free stream and boundary layer scales.

Figure 11 shows frequency spectra at different y-positions measured at $x = 500$ mm

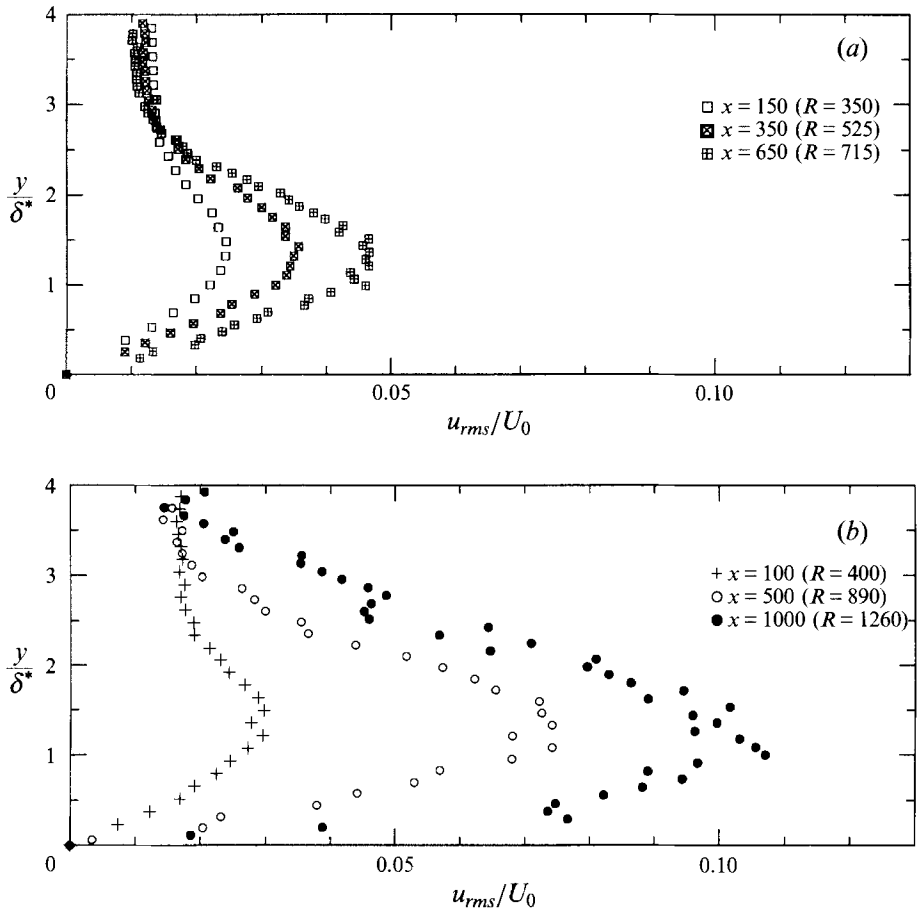

FIGURE 9. Profiles of total u_{rms} fluctuations at different R. (*a*) $U_0 = 4$ m s^{-1}, $Tu = 1.35\%$, (*b*) $U_0 = 8$ m s^{-1}, $Tu = 1.5\%$.

and $U_0 = 8$ m s^{-1}. The spectra correspond to the middle of the boundary layer (where u_{rms} is maximum), the near-wall region (where TS-waves would have their maximum), and in the free stream. Whereas the free stream energy is smoothly distributed over frequencies up to several hundred Hz, the energy distribution in the boundary layer is strongly concentrated at low frequencies, and this is seen more clearly when the wall is approached. This may be interpreted as that the boundary layer selectively amplifies low-frequency fluctuations from the free stream. Another view, which will be substantiated in the following, is that the perturbations entering the boundary layer at some upstream position are continuously elongated by the mean shear, leading to stretched structures, which are seen as low-frequency fluctuations. Higher frequencies may be the result of random motions of such structures. Suppose that the structures move at a velocity equal to the local mean velocity at $u_{rms,max}$, i.e. about $0.7U_0$. A frequency of 100 Hz at 8 m s^{-1} would then correspond to a structure with a length of 55 mm, and 10 Hz would correspond to 0.55 m, i.e. the order of x. It should also be emphasized that the previously described boundary layer disturbances are not influenced by turbulent spots. If measurements are carried out without spot sorting in the region of transition onset, the boundary layer spectra will show an increase in energy over all frequencies, and the corresponding r.m.s.-profile will show

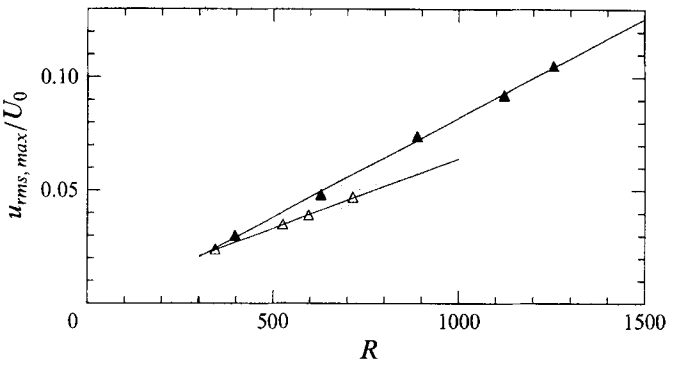

FIGURE 10. Downstream development of $u_{rms,max}$. $U_0 = 4$ m s^{-1} (△), $U_0 = 8$ m s^{-1} (▲).

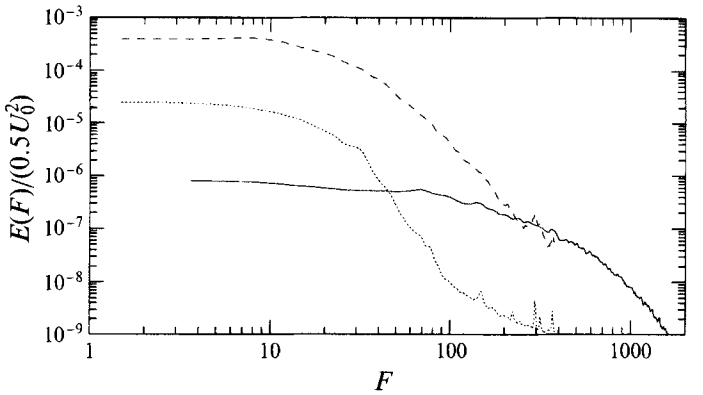

FIGURE 11. Energy density spectra for u at different wall-normal positions at $x = 500$ mm, $U_0 = 8$ m s^{-1} ($R = 890$). Free stream (—), middle of the boundary layer (– – –), near wall region (· · ·).

a large-amplitude maximum near the wall due to the turbulent spots. It should be noted that the measurements at 8 m s^{-1} in figures 9, 10 and 11 were carried out with set-up II, and could therefore be slightly affected by probe vibrations. However, a strong overestimation of the possible influence on the u_{rms}-profile at $x = 100$ mm (which is the position where the influence should be largest) gave that the increase in u_{rms} is less than 10% of the correct value close to the wall, and just a few percent at $u_{rms,max}$. In the near-wall spectra shown in figure 11, the probe vibrations can be observed as a small kink on the curve at $F = 30$ (which corresponds to $f = 20$ Hz).

Figure 12 shows profiles of the energy contributions to u_{rms} from selected narrow frequency bands, measured at $x = 500$ mm and $x = 1000$ mm for $U_0 = 8$ m s^{-1}. With increasing frequency, the energy maximum with respect to y is shifted further out in the boundary layer, which is in agreement with observations made by Kosorygin *et al.* (1982) under similar conditions. This monotonic trend suggests the existence of a specific type of structure, rather than a combination of modes. The frequency band $F = 75$ represents typical TS-wave frequencies at these Reynolds numbers, and its shape displays no special features in this context. Its maximum is in the outer part of the boundary layer, and there is no evidence of a near-wall maximum typical for TS-waves. However, this observation does not allow any conclusion about the existence or non-existence of TS-waves. At the present level of FST, it would be

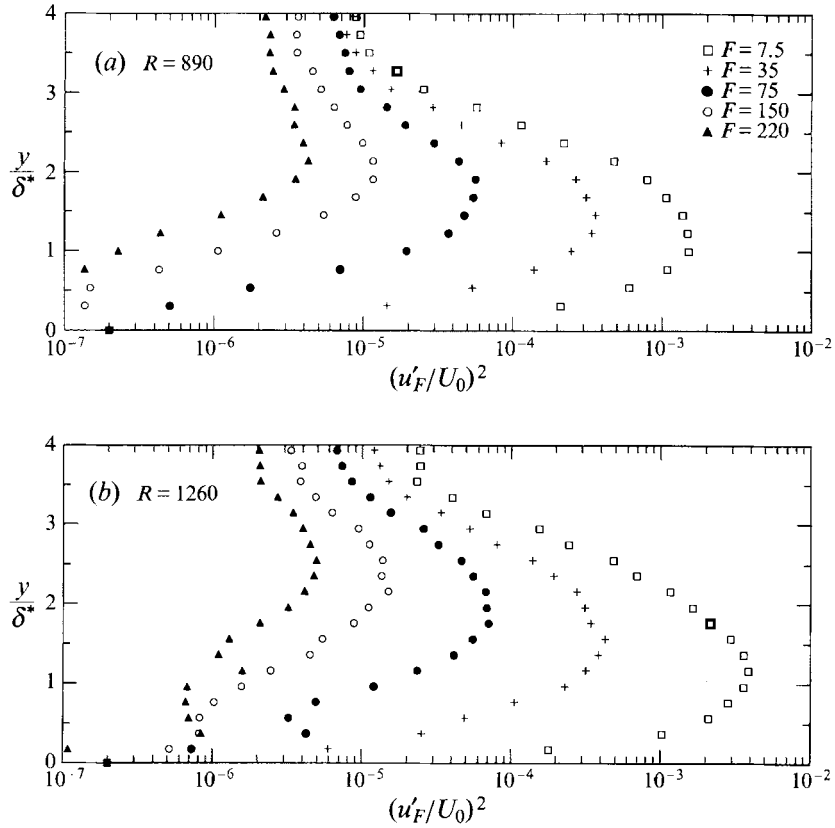

FIGURE 12. Profiles of fluctuating energy in frequency bands at $U_0 = 8$ m s^{-1}. (*a*) $x = 500$ mm, ($R = 890$), (*b*) $x = 1000$ mm ($R = 1260$).

impossible to detect naturally occurring TS-waves by merely looking at r.m.s.-spectra, since these are dominated by other fluctuations with much larger amplitudes.

As seen in figure 12, most of the energy is concentrated at low frequencies ($F \leqslant 35$), whereas the energy at higher frequencies gives only small contributions to u_{rms}. The downstream growth of u_{rms} is mainly due to an increase of energy at F below 30, whereas it is almost constant for higher frequencies. At the u_{rms}-maximum with respect to y, the energy in the band $F = 7.5$ is seen to increase by a factor of 2.6 between the two x-positions, while the corresponding increase in the total energy is only a factor of 1.4. (For comparison the free stream energy in this band is approximately constant.) Hence, energy is redistributed from high to low frequencies. If the low-frequency components are supposed to represent the motion of longitudinal streaks in the boundary layer, it means that the streaks not only grow in amplitude but also elongate as they travel downstream. The redistribution of energy to lower frequencies is seen more clearly in figure 13, which shows the ratio between the upstream and downstream energies ($E_\delta|_{x=1000}/E_\delta|_{x=500}$), where $E_\delta(F)$ is the fluctuating energy at the frequency F ($u_F'^2$) integrated through the boundary layer (δ was here taken as $4.2\delta^*$ at both positions):

$$E_\delta(F) = \frac{1}{\delta}\int_0^\delta u_F'^2 \mathrm{d}y\,.$$

The energy increases for $F \geqslant 30$, while the growth is very small for F between 30 and

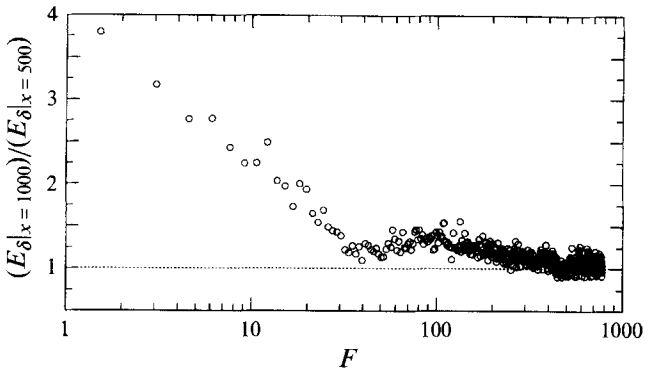

FIGURE 13. Ratio of the fluctuation energy integrated across the boundary layer at $x = 1000$ mm ($R = 1260$) and $x = 500$ mm ($R = 890$). $U_0 = 8$ m s^{-1}.

60. From oscilloscope observations, higher intermittency was observed close to the boundary layer edge. This tendency was enhanced downstream, which is seen as a slightly larger growth for $F > 60$. The same behaviour can be observed in figure 12, where the energy in frequency bands $F \geqslant 75$ shows a small downstream increase at $y/\delta^* \approx 2 - 3.5$, although the energy maxima (with respect to y) are constant at both x-positions.

The spanwise distribution of the boundary layer perturbations can be assessed by measuring the correlation between two hot wires displaced in the spanwise direction. Previous authors (cf. Kendall 1985; Kosorygin & Polyakov 1990) have observed a clear anti-correlation at a certain spanwise probe separation, approximately the size of the boundary layer thickness. Visualizations by Kendall showed spanwise streak formations separated by about twice the distance of the measured minimum in the spanwise correlation. This gives a clear indication of the existence of longitudinal streak structures in the boundary layer, and the measured scale corresponds to half of their average spacing. Figure 14 shows correlations obtained in the present set-up at $x = 500$ mm ($R = 890$) and $x = 1000$ mm ($R = 1260$), and they were measured at the y-position where u_{rms} has a maximum (the corresponding correlation in the free stream is also included for reference). The correlations attain a value of -0.3 at a spanwise separation of about 5.5 mm at $R = 890$ and 6.5 mm at $R = 1260$. This is of the order of the boundary layer thickness (4.8 and 6.8 mm at the respective x-positions), but also matches the transverse scales of the FST ($\lambda_v = 5.2$ and 5.9 mm, and $\Lambda_v \approx 7 - 10$ mm at both positions). The ratio between the spanwise scales in the boundary layer is smaller than the ratio between the boundary layer thickness at the two positions, but slightly larger than the ratio between the microscales. Hence, from the present measurements it is difficult to draw any conclusions about what determines the spanwise scales.

5. Discussion and comparison with other experiments

The results presented above will be compared with results obtained by other authors at different free stream conditions, so that further conclusions can be drawn about the parameters involved in the receptivity of the boundary layer to FST. The modification of the boundary layer mean velocity in the presence of FST was found to give an increase in the wall shear stress, and a velocity defect in the outer part of the boundary layer. Only a few authors have previously reported measurements of U

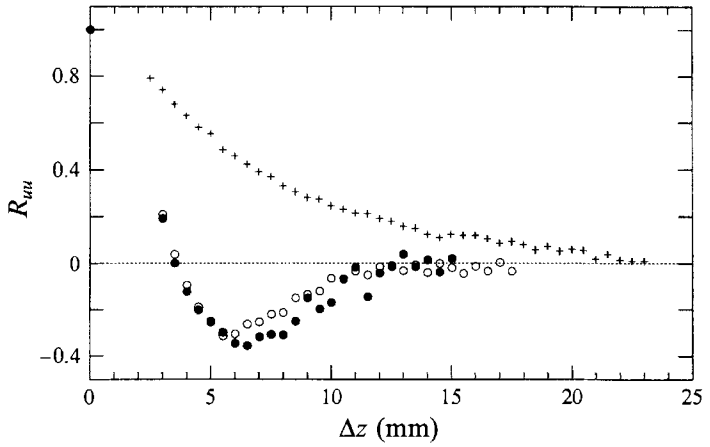

FIGURE 14. Spanwise correlations in the boundary layer, measured close to the maximum of u_{rms} for $U_0 = 8$ m s^{-1}: $x = 500$ mm ($R = 890$) (○), $x = 1000$ mm ($R = 1260$) (●). Spanwise correlation in the free stream ($x = 500$ mm) (+).

in the laminar region upstream of the onset of transition, and different observations are in disagreement. In the experiment of Kendall (1985), FST was generated with vertical rods placed in the stagnation chamber, giving a turbulence intensity Tu of 0.12% in the test section (the intensity in v was probably larger due to the suppression of u in the contraction). ΔU was evaluated from measurements made with the grid first present and then absent. Kendall reported a deviation of about 1.5%, measured at $R = 1685$. The y-distribution of ΔU given by Kendall is quite different from that found in the present experiment – it shows a velocity deficit throughout the boundary layer (not only in the outer part), which means that the wall shear stress is smaller than in the undisturbed boundary layer. The results of Roach & Brierley (1992) do not allow a direct comparison of the mean velocity profiles with and without the grid installed. However, the mean profiles obtained in the T3A and T3AM test cases ($Tu = 3\%$ and 1% respectively) were compared with a Blasius profile, showing qualitatively the same mean flow deviation as in the present experiment. Also in experiments by Dyban, Epik & Suprun (1976), carried out at different Tu ranging from 0.3% to 12%, a clear increase of the wall shear stress was observed, as well as a velocity deficit in the outer part of the boundary layer.

In the present experiment, the shape factor was found to decrease linearly with R at a rate independent of the free stream velocity. The same conclusion can be drawn by comparing the shape factors measured by Arnal & Juillen (1978) and Roach & Brierley (1992) which were measured at almost the same level of Tu (0.85% and 1% respectively), but at different U_0. Their H-values are plotted in figure 15 together with the values obtained here and those of Roach & Brierley for $Tu = 3\%$. The decrease in H within the laminar region is seen to depend mainly on Tu, and not strongly on the detailed structure of the FST.

A comparison of measurements of the fluctuations in the boundary layer with previous authors' results shows qualitative agreement. The dominance of low frequencies inside the boundary layer, as well as the downstream growth of u_{rms} have been observed by most authors, in accordance with the present results. For a large range of Tu, the u_{rms} distributions obtained in different studies have approximately the same shape, and the y-position of $u_{rms,max}$ is found to be slightly below the middle

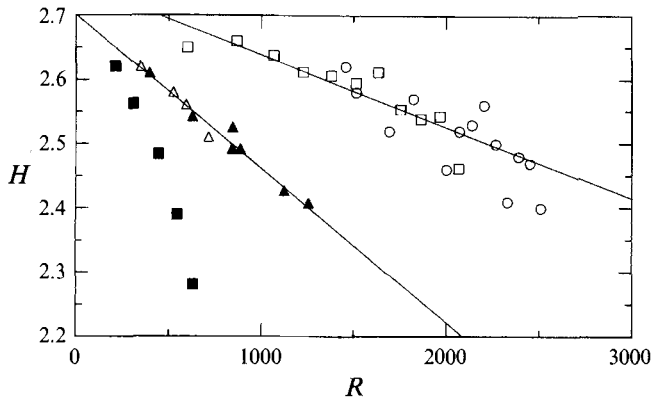

FIGURE 15. Comparison of the downstream development of the shape factor (H) in different experiments. Present results: $U_0 = 4$ m s^{-1} (△), $Tu = 1.35\%$, $U_0 = 8$ m s^{-1} (▲), $Tu = 1.5\%$. T3A (Roach & Brierley): $Tu = 3\%$ (■), $Tu = 1\%$ (□). Arnal & Juillen: $Tu = 0.85\%$ (○).

of the boundary layer. Its exact position, as well as the rate of downstream growth depends on U_0 (and thereby probably on the structure of the FST).

Inspection of the data given by Arnal & Juillen (1978), Kosorygin *et al.* (1982), and the T3A and T3AM test cases shows a linear increase of $u_{rms,max}$ with R, as also observed in the present experiments. However, when comparing results obtained with different types of FST, it is clear that there is no simple relation between the level of r.m.s.-fluctuations inside and outside the boundary layer. Figure 16 shows the variation of $u_{rms,max}/(Tu\,U_0)$ with R for the studies quoted above (i.e. the ratio between the u-fluctuations inside and outside the boundary layer). The rate of growth of this quantity, i.e. the slope of the straight lines connecting the data points for each set of measurements, is of the same order of magnitude in all experiments, showing a general trend for the growth rate of u_{rms}/U_0 to increase with Tu. However, it can be seen that different experiments with similar FST levels show quite different growth rates. Some of the parameters used in these experiments are listed in table 3, together with the approximate location of the transition onset (R_T) and the corresponding maximum in the u_{rms} level. As observed, both R_T and $u_{rms,max}$ show large differences between the experiments, although the experimental parameters are quite similar in some cases.

The existence of a well defined spanwise scale has also been observed in several studies. This scale can be interpreted as the average spacing between longitudinal structures in the boundary layer, and it would be of interest to clarify if it is determined primarily by the free stream conditions, or by some mechanism inherent to the growth of these structures inside the boundary layer. This is, however, not possible to deduce from the present data, since the spanwise scale inside the boundary layer approximately matches both the typical turbulence scales in the free stream and the boundary layer thickness. Unfortunately, this is also the case in the experiment by Kendall (1985). He presented spanwise correlation functions of u inside and outside the boundary layer at $R = 1740$. The maximum of the spanwise anti-correlation inside the boundary layer was found at $\Delta z \approx 10$ mm, and the boundary layer thickness was about 6.5 mm, which is close to the values obtained here at $R = 1260$. From the spanwise correlation of u in the free stream, the transverse scales can roughly be estimated as 4 and 5 mm (micro and macro scales respectively), which is smaller than in the present set-up. The ratio between boundary layer scales and free stream scales

	Tu (%)	M (mm)	U_0 ($m\,s^{-1}$)	R_T	$u_{rms,max}/U_0$ at R_T (%)
Arnal & Juillen (1978)					
No grid	0.12		29	2250	1.5
Grid 1	0.85	2.3	29	2450	5.5
Grid 2	1.1	3.1	29	1500	7
Roach & Brierley (1992)					
T3AM	1	4.2	19.8	2100	7.5
T3A	3	25.4	5.4	600	11
Present results					
8 $m\,s^{-1}$	1.5	23.5	8.0	> 1300	> 11
Suder *et al.* (1988)					
Grid 0.5	0.65	(22.4+screen)	30.5	1200	5.5
Grid 1	0.9	22.4	30.5	1200	6.5
Grid 2	2	65	30.5	< 850	9

TABLE 3. Comparisons of different experimental studies

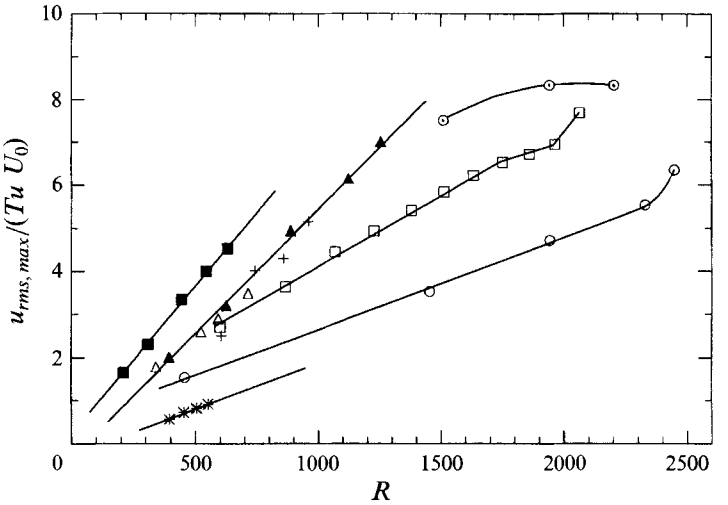

FIGURE 16. Comparison of the downstream growth of $u_{rms,max}/(Tu\,U_0)$ in different experiments. Present results: $U_0 = 4$ $m\,s^{-1}$ (△), $Tu = 1.35\%$, $U_0 = 8$ $m\,s^{-1}$ (▲), $Tu = 1.5\%$. T3A Roach & Brierley: $Tu = 3\%$ (■), $Tu = 1\%$ (□). Arnal & Juillen: $Tu = 0.85\%$ (○), $Tu = 0.12\%$ (⊙). Kosorygin *et al.*: $Tu = 1.4\%$ (+), $Tu = 3.2\%$ (*).

is then 2–2.5 compared with about 1 in the present case. The fact that similar scales were found inside the boundary layer in both experiments despite the disparity in free stream scales, indicates that there is no direct correspondence between the boundary layer and free stream scales. This is also consistent with an observation of Arnal & Juillen (1978), that the free stream turbulence is poorly correlated with the boundary layer fluctuations.

An important observation to be made from table 3 is the fact that $u_{rms,max}$ is poorly correlated with the onset of transition. This seems to indicate that the low-frequency fluctuations which dominate u_{rms} are not directly responsible for transition. It can also be seen that the value of Tu is not sufficient to predict the onset of transition. This may to some extent be due to effects which are not directly related to the free stream

turbulence itself. One such effect might be the leading edge conditions. In the present study, inappropriate leading edge conditions were found to result in a substantial upstream movement of the transition point. The pressure distribution in the presence of the grid is not reported in any of the studies quoted here, but its influence may be appreciated from the value of the shape factor. In most experiments, H is above the Blasius value at upstream positions, which can be the effect of a suction peak near the leading edge. In the experiments by Suder *et al.*, a maximum variation in C_p below 3% was reported in the region $x > 80$ mm. However, the most upstream velocity profiles in their '0.5-grid' case have shape factors above 2.7, which indicate that leading edge effects may have been a major reason for the rapid transition observed in their experiments.

6. Summary and conclusions

The above observations can be summarized as follows:

(i) The perturbations inside the boundary layer are dominated by large-scale, narrow structures, which grow downstream both in length and in amplitude. Their streamwise scale is much larger than typical longitudinal scales in the free stream. The u-perturbations, both mean (ΔU) and fluctuating (u_{rms}), have near self-similar shapes, and the peak value of u_{rms}/U_0 increases in linear proportion to R. In general the growth rate increases with Tu, but it also depends on other free stream parameters. There seems to be no direct relation between the value of u_{rms}/U_0 in the boundary layer and the point of transition onset.

(ii) The downstream increase of fluctuations inside the boundary layer leads to an increase in the Reynolds stresses, resulting in an increased wall shear stress; however, the mass flow within the boundary layer is not affected. The shape factor decreases in linear proportion to R, at a rate which depends on the overall level of the FST (i.e. Tu), but not on its detailed structure.

(iii) The spanwise scale of the boundary layer perturbations is comparable to the transverse scales in the free stream; however, no direct relation can be established from the available data. Its downstream increase is faster than that of the free stream scales, but slower than that of the boundary layer thickness.

In future experiments, it is important to give an extensive description of the free stream characteristics, in order to be able to compare the results obtained in different set-ups. With a proper estimation of the turbulent scales, for instance, it may be possible to conclude something about the spanwise scale selection mechanism by comparing the FST-scales with the scales inside the boundary layer. Experimental set-ups, in which these scales are of clearly different sizes, could be of particular interest. Since there is evidence that the boundary layer is more receptive to v- than to u-disturbances, both the u- and v-components in the free stream must be measured, in order to find correlations between the FST and transition.

The observed low-frequency structures are similar to the 'puff' observed by Grek *et al.* (1985) and the 'incipient spot' studied by Klingmann (1992) and Henningson *et al.* (1993). This similarity is not surprising, since free stream eddies entering the boundary layer may be thought of as localized transient disturbances, which develop in the same way as disturbances initially confined to the boundary layer. Transient disturbances develop into longitudinal structures inside the boundary layer with a spanwise spacing which is typically of a size comparable to the boundary layer thickness (however, the spanwise scale selection is rather weak and sensitive

to the forcing conditions). They grow downstream both in length and in amplitude, while maintaining their spanwise scale. The growth is algebraic in x (as opposed to the exponential growth of e.g. TS-waves), and is probably governed by the linear mechanism suggested by Gustavsson (1991) and Henningson *et al.* (1993) on the basis of the Orr–Sommerfeld–Squire equations. In growing boundary layers, the algebraic growth of longitudinal structures is intimately tied to the non-parallel development of the boundary layer itself. This is most comprehensively demonstrated in a recent work by Herbert (1993), and the role of this mechanism in FST-induced transition is discussed by Herbert *et al.* (1993). From the present study it is clear that the downstream development of FST-induced flow structures is also algebraic, and their spanwise scale varies more slowly than the boundary layer thickness. However, algebraic growth occurs only during a limited initial phase, and eventually the longitudinal structures decay unless the initial forcing exceeds some threshold level. This is in contrast to the continuous downstream growth in u_{rms} observed in the presence of FST. It is therefore not clear to what extent the development of the boundary layer fluctuations are due to the dynamics inside the boundary layer, and to what extent they are the result of a continuous forcing from the free stream along the boundary layer edge.

The r.m.s.-value of the low-frequency fluctuations reaches significant levels (between 5–10% before the onset of transition); however, its magnitude is poorly correlated with the onset of turbulent motion. This indicates that a transition criterion cannot be obtained only from information about the longitudinal structures in the boundary layer. The question can only be answered by taking into account different possible routes to transition and understanding their relative importance. Experiments with controlled 'model' disturbances, as well as parametric studies using theoretical and numerical models, are therefore necessary. An attempt in this direction is made in an accompanying paper (Boiko *et al.* 1994), where the role of the Tollmien–Schlichting wave instability in the present flow is investigated.

This work was supported by the Swedish National Board for Industrial and Technical Development (NUTEK), and the Swedish Research Council for the Engineering Sciences (TFR). The visits of Professor V.V. Kozlov and Dr A.V. Boiko to Stockholm and the visit of Dr B.G.B. Klingmann to Novosibirsk were made possible through the scientific exchange program sponsored by the Royal Swedish Academy of Sciences (KVA) in cooperation with the Russian Academy of Sciences. The data obtained by Roach & Brierley at Rolls-Royce were generously put at our disposal by Dr J. Coupland.

Appendix

The Falkner–Skan (FS) profile is obtained by assuming that the free stream velocity varies as $U_0 \sim (x - x_0)^m$, and the FS parameter m is directly related to C_p by

$$m = \frac{-1}{2(1 - C_p)}(x - x_0)\frac{\partial C_p}{\partial x}.$$

x_0 is a virtual origin, which can be determined by comparing the measured displacement thickness (δ^*) with the theoretical one. The FS flow is a self-similar solution to the boundary layer equations, using the similarity coordinate

$$\eta = \frac{y}{[\nu(x - x_0)/U_0]^{1/2}}$$

and the shape factor H is uniquely determined by m. For example, $H = 2.53$ (the value measured with the grid at $x = 450$ mm for $U_0 = 8.1$ m s^{-1}), corresponds to $m = 0.026$, which is a FS profile with $y/\delta^* = 1.59\eta$. The measured value of δ^* is 1.553 mm, giving a virtual origin $x_0 = -65$ mm. The negative pressure gradient corresponding to this FS profile is then $\partial C_p/\partial x = -0.1$ m^{-1}.

REFERENCES

ARNAL, D. 1992 Transition description and prediction. In *Numerical Simulation of Unsteady Flows and Transition to Turbulence* (ed. O. Pironneau, W. Rodi, I. L. Ryhming, A. M. Savill & T. V. Truong), pp. 303–316. Cambridge University Press.

ARNAL, D. & JUILLEN, J. C. 1978 Contribution expérimentale à l'etude de la receptivité d'une couche limite laminaire, à la turbulence de l'écoulement general. *ONERA Rapport Technique* No 1/5018 AYD, June 1978.

BAINES, W. D. & PETERSEN, E. G. 1951 An investigation of flow through screens. *Trans. ASME* **73**, 467–480.

BLAIR, M. F. 1992 Boundary-layer transition in accelerating flows with intense freestream turbulence: Part 1 – Disturbances upstream of transition onset. *Trans. ASME* I: *J. Fluids Engng.* **114**, 313–321.

BOIKO, A. V., WESTIN, K. J. A., KLINGMANN, B. G. B., KOSLOV, V. V. & ALFREDSSON, P. H. 1994 Experiments in a boundary layer subjected to free stream turbulence. Part 2. The role of TS waves in the transition process. *J. Fluid Mech.* **281**, 219–245.

BREUER, K. S. & LANDAHL, M. T. 1990 The evolution of a localized disturbance in a laminar boundary layer. Part 2. Strong disturbances. *J. Fluid Mech.* **220**, 595–621.

DYBAN, YE. P., EPIK, E. YA. & SUPRUN, T. T. 1976 Characteristics of the laminar boundary layer in the presence of elevated free-stream turbulence. *Fluid Mech. - Sov. Res.* **5**(4), 30–36.

GREK, H. R., DEY, J., KOZLOV, V. V., RAMAZANOV, M. P. & TUCHTO, O. N. 1991 Experimental analysis of the process of the formation of turbulence in the boundary layer at higher degree of turbulence of windstream. *Rep. 91-FM-2, Indian Inst. Science, Bangalore, 560012, India.*

GREK, H. R., KOZLOV, V. V. & RAMAZANOV, M. P. 1985 Three types of disturbances from the point source in the boundary layer. In *Laminar-Turbulent Transition 2* (ed. V. V. Kozlov), pp. 267–272. Springer.

GROTH, J. & JOHANSSON, A. V. 1988 Turbulence reduction by screens. *J. Fluid Mech.* **197**, 139–155.

GULYAEV, A. N., KOZLOV, V. E., KUZNETSOV, V. R., MINEEV, B. I. & SEKUNDOV, A. N. 1989 Interaction of a laminar boundary layer with external turbulence. *Izv. Akad. Nauk SSSR, Mekh. Zhid. Gaza* **5**, 55–65 (in Russian, English transl. 1990 in *Fluid Dyn.* **24**:5, 700–710).

GUSTAVSSON, L. H. 1991 Energy growth of three-dimensional disturbances in plane Poiseuille flow. *J. Fluid Mech.* **224**, 241–260.

HENNINGSON, D. S., LUNDBLADH, A. & JOHANSSON, A. V. 1993 A mechanism for bypass transition from localized disturbances in wall-bounded shear flows. *J. Fluid Mech.* **250**, 169–207.

HERBERT, T. 1993 Studies of boundary layer receptivity with parabolized stability equations. *AIAA Paper* 93-3053.

HERBERT, T., STUCKERT, G. K. & ESFAHANIAN, V. 1993 Effects of free-stream turbulence on boundary layer transition. *AIAA Paper* 93-0488.

HINZE, J. O. 1975 *Turbulence*, 2nd Edn. McGraw-Hill.

JOHANSSON, A. V. 1992 A low speed wind-tunnel with extreme flow quality — design and tests. In *Proc. ICAS Congress 1992. Paper* ICAS-92-3.8.1, pp. 1603–1611. ICAS/AIAA.

KENDALL, J. M. 1985 Experimental study of disturbances produced in a pre-transitional laminar boundary layer by weak freestream turbulence. *AIAA Paper* 85-1695.

KENDALL, J. M. 1990 Boundary layer receptivity to freestream turbulence. *AIAA Paper* 90-1504.

KENDALL, J. M. 1991 Studies on laminar boundary layer receptivity to freestream turbulence near a leading edge. In *Boundary Layer Stability and Transition to Turbulence* (ed. D. C. Reda, H. L. Reed & R. Kobayashi), *ASME FED* **114**, 23–30.

KLINGMANN, B. G. B. 1992 On transition due to three-dimensional disturbances in plane Poiseuille flow. *J. Fluid Mech.* **240**, 167–195.

KLINGMANN, B. G. B., BOIKO A. V., WESTIN, K. J. A., KOZLOV, V. V. & ALFREDSSON, P. H. 1993 Experiments on the stability of Tollmien-Schlichting waves. *Eur. J. Mech./ B Fluids* **12**, 493–514.

KOSORYGIN, V. S. & POLYAKOV, N. PH. 1990 Laminar boundary layers in turbulent flows. In *Laminar-Turbulent Transition 3* (ed. D. Arnal & R. Michel), pp. 573–578. Springer.

KOSORYGIN, V. S., POLYAKOV, N. PH., SUPRUN, T. T. & EPIK, E. YA. 1982 Development of disturbances in the laminar boundary layer on a plate at a high level of free stream turbulence. In *Instability of Subsonic and Supersonic Flows*, pp. 85–92. Institute of Theoretical and Applied Mechanics, Siberian Branch of USSR Academy of Sciences, Novosibirsk (in Russian).

KOZLOV, V. E., KUZNETSOV, V. R., MINEEV, B. I. & SEKUNDOV, A. N. 1990 The influence of free-stream turbulence and surface ribbing on the characteristics of a transitional boundary layer. In *Near-Wall Turbulence, Proc. of 1988 Zorian Zaric Mem. Conf.* (ed. S. J. Kline & N. H. Afgan), pp. 172–189. Hemisphere.

PIRONNEAU, O., RODI, W., RYHMING, I. L., SAVILL, A. M. & TRUONG, T. V. 1992 *Numerical Simulation of Unsteady Flows and Transition to Turbulence.* Cambridge University Press.

ROACH, P. E. & BRIERLEY, D. H. 1992 The influence of a turbulent free-stream on zero pressure gradient transitional boundary layer development. Part I: Test cases T3A and T3B. In *Numerical Simulation of Unsteady Flows and Transition to Turbulence* (ed. O. Pironneau, W. Rodi, I. L. Ryhming, A. M. Savill & T. V. Truong), pp. 319–347. Cambridge University Press.

SUDER, K. L., O'BRIEN, J. E. & RESHOTKO, E. 1988 Experimental study of bypass transition in a boundary layer. *NASA Tech. Mem.* 100913.

YANG, Z. Y. & VOKE, P. R. 1991 Numerical simulation of transition under turbulence. *University of Surrey, Dept. Mech. Eng. Rep. ME-FD*/91.01.